frontiers in Energy Research

ORIGINAL RESEARCH
published: 29 January 2021
doi: 10.3389/fenrg.2020.615677

$Na_{0.44}MnO_2$/Polyimide Aqueous Na-ion Batteries for Large Energy Storage Applications

*Satyanarayana Maddukuri, Amey Nimkar, Munseok S. Chae, Tirupathi Rao Penki, Shalom Luski and Doron Aurbach**

Department of Chemistry and BINA (BIU Center for Nano-Technology and Advanced Materials), Bar-Ilan University, Ramat-Gan, Israel

Aqueous salt batteries with high concentrations of salt or water in salt aqueous systems have received considerable attention with focus on improving working voltage range and energy density. Here, the effect of $NaClO_4$ salt concentration on the electrochemical performance and stability of tunnel-type $Na_{0.44}MnO_2$ (NMO) cathodes and organic polyimide (PI) derivative anodes was studied. High capacity retention and 100% coulombic efficiency were shown for NMO/PI full cell in saturated $NaClO_4$ electrolyte. A high, stable capacity of 115 mAh/g was achieved for the PI anode material, and the full cell showed a stable capacity of 41 mAh/g at 2C rate for 430 cycles (calculated for the weight of NMO cathode). Even at a fast 5C rate, a discharge capacity of 33 mAh/g was maintained for 2,400 prolonged cycles with nearly 100% efficiency. The full cell device can achieve an average voltage of 1 V with energy density of 24 Wh/kg. This study highlights concentrated sodium perchlorate as a promising electrolyte solution for stabilization of electrodes and enhancement of electrochemical performance in aqueous media.

Keywords: aqueous Na-ion batteries, water in salt electrolytes, intercalation materials, aqueous batteries, polyimide anodes

OPEN ACCESS

Edited by:
Zhumabay Bakenov, Nazarbayev University, Kazakhstan

Reviewed by:
Almagul Mentbayeva, Nazarbayev University, Kazakhstan
Yuesheng Wang, Hydro-Québec's Research Institute, IREQ, Canada
Fudong Han, Rensselaer Polytechnic Institute, United States

****Correspondence:***
Doron Aurbach
Doron.Aurbach@biu.ac.il

Specialty section:
This article was submitted to Electrochemical Energy Conversion and Storage, a section of the journal Frontiers in Energy Research

Received: *09 October 2020*
Accepted: *15 December 2020*
Published: *29 January 2021*

Citation:
Maddukuri S, Nimkar A, Chae MS, Penki TR, Luski S and Aurbach D (2021) $Na_{0.44}MnO_2$/Polyimide Aqueous Na-ion Batteries for Large Energy Storage Applications. Front. Energy Res. 8:615677. doi: 10.3389/fenrg.2020.615677

INTRODUCTION

Electrochemical devices for large energy storage are in high demand and the technologies based on batteries as well as capacitors are explored. Commercial batteries are working on high energy and low power density with low rate capability, while capacitors combine low energy and high power density with high rate capability (Barbieri et al., 2005; Armand and Tarascon, 2008; Poonam et al., 2019). Due to the increased use of nonaqueous Li ion batteries in mobile electronics and electric vehicles, capacity-based systems have emerged, offering low-cost devices with pure adsorption and desorption of ions at the electrode surface, a nonfaradaic mechanism that delivers a low energy density of 10 Wh/kg (Simon and Gogotsi, 2008). In organic and ionic liquid-based electrolyte solution, capacitors allow operation of devices even at high voltage around 3 V with increased energy density (Brandt et al., 2013; Brandt and Balducci, 2014; Yu and Chen, 2019). Large energy storage requires safe, cheap, and environmentally friendly materials. Lead acid batteries are used in commercial devices with good energy density of 40 Wh/kg; however, the failure of lead acid battery related with low discharge efficiency, usage of toxic lead, highly corrosive nature of acidic electrolyte which leads to search for alternative technologies (Yolshina et al., 2015; Yang et al., 2017b; Sadeghi and Javaran, 2019). Devices based on aqueous electrolytes have proved to be safer in spite of low energy production compared to nonaqueous systems.

In order to achieve a low-cost device with high capacity, rate capability, and efficiency, one needs to consider components such as current collectors, electrolytes, and electrode materials. Sodium-based electrolytes are cheaper than lithium-based electrolytes, owing to the abundant nature of sodium vs. lithium salts in the earth's crust. In general, chemically modified or coated metal grid/sheets are used as current collectors for studying aqueous batteries. For example, aluminum, stainless steel, and nickel foil current collectors are handicapped by their highly corrosive nature in aqueous systems (Li and Church, 2016; Li, 2017). Gheytani et al. explored a chromate conversion–coated Al collector for aqueous Li ion batteries (Gheytani et al., 2016). Carbon-coated stainless steel mesh was investigated for corrosion resistance in aqueous media (Wen et al., 2017). In order to avoid the high toxicity of chromium, to reduce coating thickness, and to maintain electrodes' uniformity during prolonged cycling, it is important to develop flexible, corrosion-resistive, and conductive composite foils as current collectors and cases. Recent studies presented some attractive energy storage devices for power supply including low-cost, nontoxic, lightweight, flexible, and wearable batteries' components (Li et al., 2014a; Yang et al., 2017a). Graphene and CNT fibers were explored for Li ion batteries and capacitor applications (Li et al., 2012; Kim et al., 2013). Such composites should contain conductive polymeric matrices that can exhibit high mechanical strength and flexibility. Tang et al. showed electrically conductive and mechanically stable current collectors made by self-assembly of CNT and RGO/polystyrene composites (Tang et al., 2014). Full cells studies of aqueous Li ion battery systems using polyimide (PI)/LMO couples showed a stable capacity at a high current rate of 20C with capacity retention of 95% after 500 cycles using stretchable carbon filler/polymer composites as current collectors (Song et al., 2018). Evanko et al. also demonstrated carbon black/polyethylene composite as corrosion-resistant collectors for stationary Zn/Br_2 aqueous batteries. These current collectors demonstrated a high overpotential for hydrogen evolution, compared to stainless steel (SS), Ti, Ni, and a high overpotential for O_2 evolution compared to SS and Ni in neutral, acidic, and basic electrolyte solutions (Evanko et al., 2018). Other types of conductive vinyl films (z-flo® 2267P) were explored for aqueous and nonaqueous supercapacitors, using aqueous KOH solutions and solutions containing tetraethylammonium tetrafluoroborate in propylene carbonate, with working voltage ranges of 0–1 and 0–2.7 V, respectively (Stoller et al., 2008; Kang et al., 2019). We also analyzed such conductive vinyl films (abbreviated as PW, which means polymeric web) as current collectors and case materials in aqueous and nonaqueous solutions.

Taking into account the abundance of elements and cost-effectiveness, we explored manganese oxides as attractive cathode materials in batteries for large energy storage applications. $Mn_3O_4/NaTi_2(PO_4)_3$ cells and symmetric devices comprising Mn_3O_4 electrodes were investigated, using aqueous Na_2SO_4 electrolyte solutions (Cao et al., 2018). Cells comprising λ-MnO_2 cathodes and capacitive activated carbon anodes with 1 M Na_2SO_4 solutions could be charged up to 2.2 V and deliver a specific energy density of 19.5 Wh/kg (Shin et al., 2020). A study of cells comprising $K_xMnO_2.xH_2O$ cathodes using Li^+, Na^+, and K^+ salts solutions exhibited high capacity, efficiency, and prolonged cycle life due to contributions of both redox and nonfaradaic adsorption/desorption interactions (Shao et al., 2013). The performance of MnO_2 was explored in different nitrate-based electrolyte solutions including $Zn(NO_3)_2$, $Mg(NO_3)_2$, $Ba(NO_3)_2$, and $Ca(NO_3)_2$ (Xu et al., 2009a). Xu et al. reported insertion and de-insertion of Zn^{2+} ions in MnO_2 electrodes using 0.1 M $Zn(NO_3)_2$ electrolyte solutions (Xu et al., 2009b). Tunnel-type $Na_{0.44}MnO_2$ (NMO) material was found to be conducive for sodium aqueous and nonaqueous batteries in terms of stability and rate capability, due to its unique structure that allows fast solid-state diffusion of relatively large Na ions. NMO material can deliver a specific capacity of around 45 mAh/g with existence of fast Na ion diffusion coefficient (within the range of $10^{-}11–10^{-12}$) (Whitacre et al., 2010). In nonaqueous media, the diffusion coefficient was lower, in the range of 10^{-14}–10^{-16} cm^2 s^{-1} (Bin et al., 2018).

In order to benefit from NMO as a cathode material for large energy storage applications, it is important to couple it with anode materials that are highly stable at the necessary low potential regions, demonstrating fast rate capability in aqueous media. NASICON-type $NaTi_2(PO_4)_3$ anode in aqueous systems has the advantage of high capacity over fully capacitive carbon materials but is handicapped by poor cycling performance as a result of low electronic conductivity, dissolution of Ti ions, and voltage limitation of aqueous electrolytes (Li et al., 2014b). Other anodes for aqueous devices were recently explored that take advantage of the low cost, easy production, and possible multi-electron transfer of organic molecules and polymers within the limits of water decomposition. Chemical modification of carbon materials with functionalized groups allowed for the delivery of high energy density for prolonged cycles. AC and Kynol cloth with electrochemically active anthraquinone and catechol showed enhanced capacitance, attributed to the redox phenomena of the attached moieties with association/dissociation of ions during discharge/charge (Pognon et al., 2011; Pognon et al., 2012; Weissmann et al., 2012; Comte et al., 2015). Anthraquinone-functionalized kynol showed association and dissociation of protons in aqueous H_2SO_4 with enolization of carbonyl groups, exhibiting a 2.5-fold increase in capacity of the modified carbon material (65 vs. 25 mAh/g); however, commercial application needs to address detachment of redox-active groups (Malka et al., 2019).

Robust organic polymer materials with stable structure are extensively studied for both aqueous and nonaqueous systems. The issue of dissolution of small organic molecules in electrolyte solutions is mitigated by using polymeric materials, thus improving the life cycle of the batteries. These polymeric electrode materials are economically viable and environmentally benign. Such polymeric functional compounds offer improved aqueous battery devices (Haüpler et al., 2016; Bhosale et al., 2018; Hernández et al., 2018). Polyimides (PIs) in aqueous Li-ion batteries demonstrated a stable capacity performance with 95% capacity retention for 1,000 cycles at 2C rate (Chen et al., 2015). PI anode material

explored by Chen et al. for Mg-aqueous ion battery using Prussian blue cathode and Mg^{2+} containing electrolyte solution showed excellent cycling performance, delivering an energy density of 40 Wh/kg. (Chen et al., 2017).

Here, a Na ion aqueous battery device for large energy storage applications is presented using tunnel-type $Na_{0.44}MnO_2$ (NMO) cathode and organic PI anode materials. The stability and performance of NMO is demonstrated as intercalation/de-intercalation cathode in different concentrations of $NaClO_4$ electrolyte solution using flexible polymeric web (PW) substrate as a current collector. We studied the polyimide derivative as anode and demonstrated the high capacity retention performance in saturated $NaClO_4$ electrolyte solution. We propose in our study that the full cells comprising NMO and PI as electrodes with an aqueous electrolyte solution can demonstrate high performance as a fast energy conversion device for load leveling and large energy storage applications.

MATERIALS AND METHODS

Material Synthesis and Electrodes Preparation

1,4,5,8-naphthalenetetracarboxylic dianhydride (NTCDA)-derived PI polymer was prepared according to the procedure reported in the literature (Song et al., 2010; Chen et al., 2014; Dong et al., 2016). Equimolar quantities of NTCDA (Apollo Scientific) and ethylene diamine (Alfa Aesar Ltd.) were added to 1-methyl-2-pyrrolidone and the reaction mixture was refluxed for 6 h by stirring. Solid residue was filtered, washed several times with ethanol, and dried in air at 120°C for 12 h. The product was heated at 300°C under nitrogen atmosphere for 8 h to complete the imidization and remove residual solvent. The purity of NMO (NEI Co. Ltd.) was determined by powder X-ray diffraction (XRD) analysis. Conductive vinyl film (Polymeric web) was used as current collector and case (purchased from Transcontinental Ltd.).

Electrode materials were dried overnight at 100°C in air, prior to electrode preparation. The weight percentage of active material, conductive agent, and binder in the cathode and anode was 75:15:10 and 60:30:10, respectively. Acetylene black and graphene (XG-Sciences) in 50:50 ratio were jointly used as a conductive agent for improving PI conductivity. The AC-based counter electrode (CE) consisted of 80:10:10 AC: acetylene black: PTFE binder (60% PTFE dispersed in water, Sigma Aldrich). The electrode composite was ball-milled at 200 rpm for 2 h using isopropanol as a solvent with the electrode material to balls weight ratio of 1:20 (7 mm dia, zirconia oxide balls were used). The obtained composite was then pressed in order to make flexible thin electrodes using a rolling machine. We reached the required size and then dried overnight at 80°C. The thickness range of the electrodes was 300–400 μm for both NMO and PI, an area of 15*15 mm for full cells study. The thickness range of electrodes was 100 and 700–800 μm for NMO or PI and activated carbon electrodes, respectively, for three electrodes cells characterization. The electrodes are cut into 15*15 mm for full cells analysis. The sizes of the electrodes were in the range of 10*10 mm for three electrodes cells analyses with excess in counter electrode. The electrodes were loaded on the PW matrices using an adhesive Graphene conductive ink (obtained from XG-sciences, in order to have a better contact) and then dried at 70°C overnight. The cells including cathode, anode, and NKK separator between them were pressed and closed by nonconductive adhesive tape (obtained from 3M™ Adhesive 300LSE) after adding a few drops of electrolyte solution. The weight of the working electrode (WE) in three-electrode cell measurements was 7.5–8.5 mg for both PI and NMO. The specific surface area was around 27 and 9 mg/cm^2 for the cathode and anode materials, respectively, used in full cells analysis.

Physical and Electrochemical Characterization

The WE and CE were dried overnight at 100°C and subjected to electrochemical analysis. Electrochemical measurements were carried out in homemade pouch-type cells for 3-electrode measurements and cells for 2-electrode measurements. A polymeric web was used as case and current collector for making pouch-type cells with NKK paper as a separator and Ag/Ag_2SO_4 as RE. Homemade aqueous electrolyte solutions were prepared with 1, 8 m and saturated $NaClO_4$. We believe that the choice of this electrolyte is good because the potential window of its aqueous solutions is wide, the safety features of its aqueous solutions are appropriate for battery applications, and it is a good choice in terms of cost-effectiveness. The electrolyte solutions were purged under N_2 atmosphere for 2 h before use for cells preparation, in order to remove dissolved oxygen. Galvanostatic charge–discharge characterization, CV, and self-discharge measurements were performed with a Bio-Logic computerized instrument. Powder XRD measurements were performed with a Bruker AXS D8 Advance diffractometer and the obtained patterns were refined using GSAS Rietveld refinement software (Toby, 2001). Morphology images were obtained by high-resolution scanning electron microscopy (HRSEM) using a JEOL-JEM-2011 (200 kV) Oxford instrument. Inductively coupled plasma-optical emission spectroscopy (ICP-OES) analysis of manganese dissolution in separators and electrolytes was carried out using a Spectro Arcos ICP-OES MultiView FHX22. The synthesized PI was characterized by Fourier-transform infrared spectroscopy (FTIR, Thermo Scientific SMART iTX).

RESULTS AND DISCUSSION

The Current Collector Stability in $NaClO_4$ Electrolyte Solutions

The photographic images of the polymeric web substrates used as current collectors (**Figure 1A,B**) show that they can be bent or twisted for device flexibility. HRSEM images of PW (**Figure 1C,D**) and CVs with different $NaClO_4$ electrolyte concentrations and Ag/Ag_2SO_4 as Pseudo reference (RE) show that the PW substrates are highly stable in the potential range of

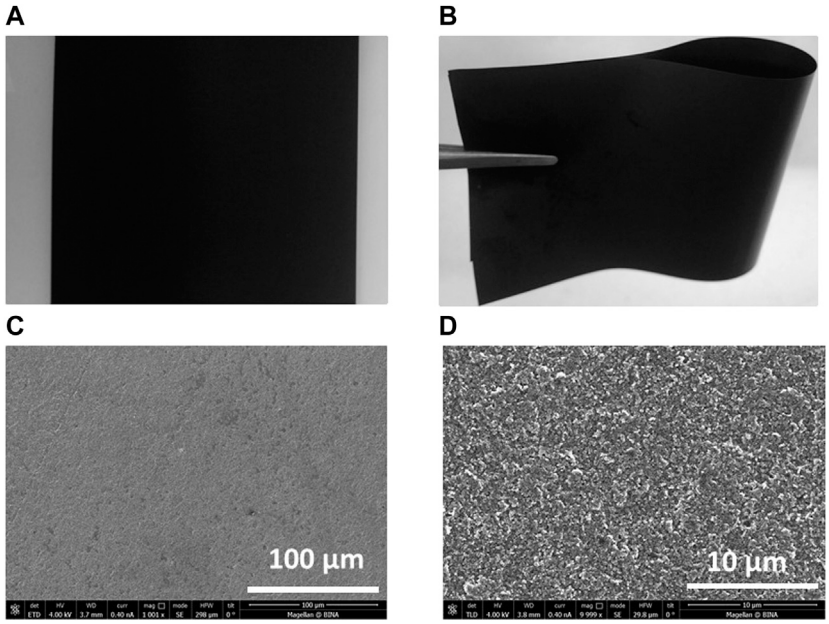

FIGURE 1 | Photographic images of the polymeric web **(A)** flat and **(B)** bent polymeric web and HRSEM images at ranges of **(C)** 100 µm at 1 k magnification and **(D)** 10 µm at 10 k magnification.

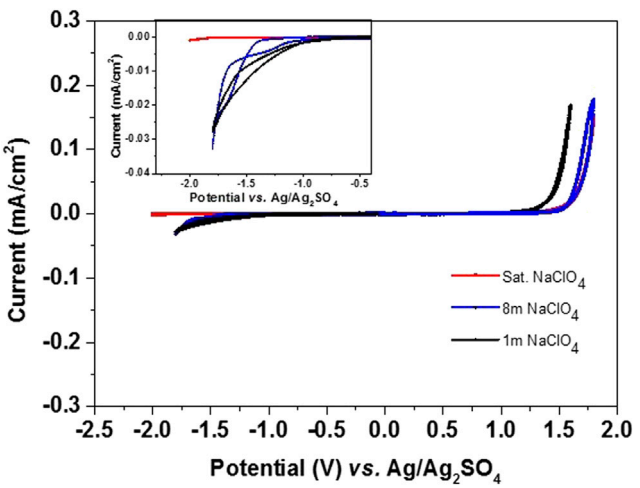

FIGURE 2 | CVs of the polymeric web substrate (case and current collector) at 1 mV/s scan rate with Ag/Ag_2SO_4 RE and 1 m (pink), 8 m (blue), and saturated (red) $NaClO_4$ electrolyte solution. The inset in the figure shows the enlarged area of the negative potential range.

−2.0 and 1.5 V vs. Ag/Ag_2SO_4 without observing any hydrogen and oxygen evolution during polarization in this potential rage in saturated NaClO4 electrolyte medium (**Figure 2**). The results indicate that the full cell charging voltage can be extended to 3.5 V using this electrolyte solution. The stability was also analyzed at electrolyte concentrations of 1 and 8 m $NaClO_4$, as shown in **Figure 2**. The stability of the less concentrated solutions is limited to −1.1 V and 1.2 vs. Ag/Ag_2SO_4 at the negative and positive edges, respectively (due to hydrogen and oxygen evolution reactions). One would think that Na_2SO_4, $NaNO_3$ NaCl, or CH_3COONa are preferable than $NaClO_4$ due to their lower cost (Lee et al., 2019). However, based on previous studies (Kim et al., 2014; Wang et al., 2015), it is possible to conclude that from an electrochemical point of view $NaClO_4$ is the best choice (as we mentioned above). As analyzed by Lee *et al.*, the highly concentrated sodium perchlorate electrolyte solution showed extended voltage ranges without decomposition relating to H_2 and O_2 evolution, due to the low concentration of the free water molecules in solution, as identified by Raman spectroscopic analysis (Lee et al., 2019). Taking into account their high stability, we used these flexible substrates in our aqueous battery studies for both electrode material characterization and devices fabrication.

Study of NMO Electrodes in $NaClO_4$ Electrolyte Solutions

The obtained Powder XRD patterns of NMO samples were refined by Rietveld analysis using GSAS, in order to verify the formation of an orthorhombic phase with the space group *Pbam*. As presented in **Figure 3A**, the measured patterns' peaks were well matched (in red color) with the calculated peaks (in green color) and the fitting parameter values were R_p = 0.017, R_{wp} = 0.028, R_{exp} = 0.011, $R(F^2)$ = 0.13086, χ^2 = 5.905, as shown in **Figure 3A**. The refined lattice parameter values are a = 9.0815(3) Å, b= 26.455(1) Å, and c = 2.8244(1) Å, in agreement with report literature (Sauvage et al., 2007; Pang et al., 2014). HRSEM images

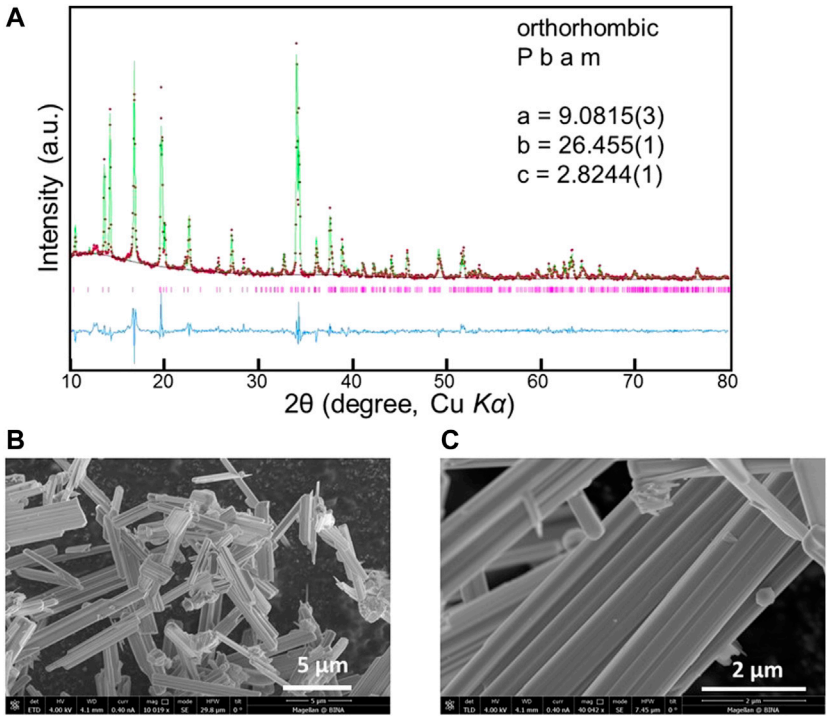

FIGURE 3 | (A) Powder XRD Rietveld refinement profile for $Na_{0.44}MnO_2$ (red points: experimental data. green line: calculated data. blue line: difference. pink bars: Bragg positions). **(B)** HRSEM images at magnification of ×10k at 5 µm range and **(C)** ×40k at 2 µm range.

of NMO are presented in **Figure 3B,C**, showing needle-shape particles. These particles are distributed with different lengths from 1 to 5 µm and are arranged in an agglomerated fashion.

In order to evaluate the electrochemical stability, the NMO electrodes were tested in 3-electrodes cells using activated carbon (AC) counter electrodes in enough excess of active mass, and Ag/Ag_2SO_4 as RE. The effect of $NaClO_4$ electrolyte concentration was studied by voltammetry using electrolyte solutions with 8m and saturated $NaClO_4$ as shown in **Figure 4** and **Figure 5**, respectively. The applied potential window was 0–0.8 V vs. Ag/Ag_2SO_4 for 20 cycles at a scan rate of 0.1 mV/s (**Figure 4A,B** and **Figure 5A,B**). The anodic and cathodic profiles show three redox peaks at potentials of 0.17/0.09, 0.40/0.32, and 0.62/0.55 V vs. Ag/Ag_2SO_4 using 8m $NaClO_4$ electrolyte, which correlate well with the reported literature (Tekin et al., 2017; Lim et al., 2018). The initial anodic capacity is 50 mAh/g with extraction of nearly 0.18 Na ions from the NMO lattice. At the end of 20 cycles, the observed discharge capacity was 35.7 mAh/g with 80% retention and a coulombic efficiency was 98%. **Figure 4C** demonstrates the CV curves at 0.5 mV/sec scan rate after scanning at 0.1 mV/s (see in **Figure 4A**). At this rate, a stable discharge capacity of 29 mAh/g was observed with an efficiency of 99% up to 50 cycles as shown in **Figure 4**. **Figure 5** shows a similar voltammetric profile with saturated $NaClO_4$ solution and redox couples at potentials of 0.21/0.12, 0.45/0.34, and 0.68/0.58 V vs. Ag/Ag_2SO_4. A stable discharge capacity of 45 mAh/g was observed after 20 cycles at slow scan rates, with a coulombic efficiency of 99.5%. Scanning was continued at 0.5 mV/s up to 50 cycles, resulting in a stable discharge capacity of 38 mAh/g. High discharge capacity and very good capacity retention were observed with the saturated electrolyte solution. These are attributed to the favorable electrodes and their interfacial stability, better charge transfer kinetics, very low content of oxygen contamination in the concentrated electrolyte solution. The advantage of concentrated solutions related to low level of dissolved oxygen was confirmed (Luo et al., 2010; Li et al., 2017).

Focusing on the high capacity and stability of NMO with concentrated electrolyte solutions, cathodes samples were stored with 8 m and saturated $NaClO_4$ solutions at 60° C for one week, then filtered and heated for drying at 100°C overnight before XRD analysis. The XRD patterns of the aged samples clearly matches with that of the parent material, showing very minor impurity peaks of Mn_2O_3 and $NaClO_4$ (as marked in **Figure 6**). The inset in the figure shows that the peak positions are nearly the same, without change in 2θ positions, and clear separation of the (0 10 0) and (3 5 0) peaks for both samples, indicating no observable loss of sodium ions from the lattice. The treatment of NMO in distilled water for one week leads to displacement of Na^+ ions with protons, resulting in a merge of the (0 10 0) and (3 5 0) peaks with lattice shrinkage of the unit cell (Dall'Asta et al., 2017).

In order to assess the contribution of Mn dissolution to capacity loss, cells were dismantled, and ICP analysis was conducted for Mn ions that present in the separators and the electrolyte solutions. The saturated electrolyte solution from cycled cells showed very minor Mn dissolution of 0.0298 µg/ml while the 8 m $NaClO_4$ electrolyte solution displays much higher Mn dissolution of about 0.306 µg/ml. These results

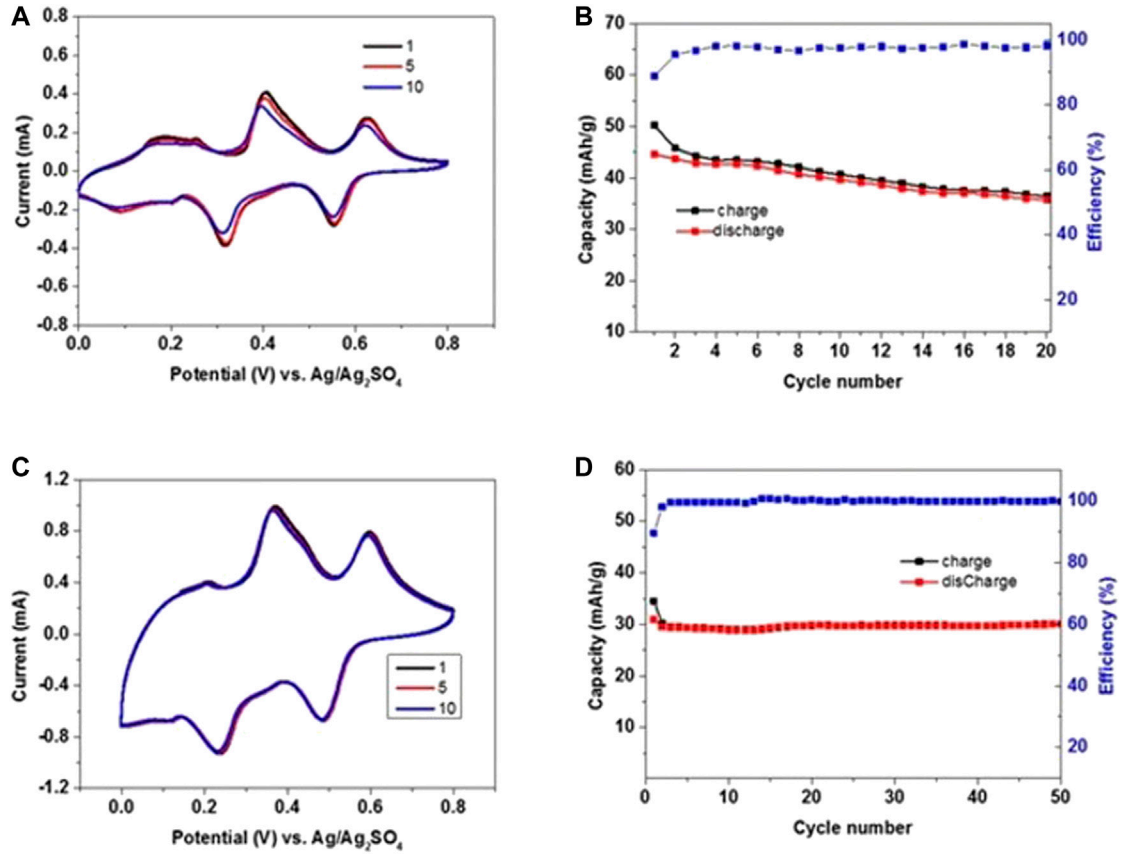

FIGURE 4 | CVs of $Na_{0.44}MnO_2$ WE and AC-rich CE in three-electrode cell configuration (electrodes were pressed onto a polymeric web current collector) in 8 m $NaClO_4$ electrolyte solution and Ag/Ag_2SO_4 RE **(A)** measured at a scan rate of 0.1 mV/s up to 20 cycles in the voltage window of 0–0.8 V vs. Ag/Ag_2SO_4 **(B)** Corresponding charge and discharge values in mAh/g during anodic and cathodic scan, respectively. **(C)** The scan rate is increased to 0.5 mV/s after 20 cycles within the same voltage range. **(D)** Charge and discharge values up to 50 cycles at 0.5 mV/s.

show that the use of highly concentrated solutions increases the stability of such types of transition metal oxide electrodes and mitigates detrimental phenomena such as dissolution of transition metal cations.

The Study of Polyimide as an Anode Material in $NaClO_4$ Electrolyte Solutions

The synthesized solid PI polymer was characterized by FTIR to confirm the structure (**Figure 7**), showing the expected bands for vibrations of imide C-N and naphthalene unit at 1349 and 1581 cm^{-1}, respectively; bands for imide vibration (C=O) at 768 cm^{-1} were found along with asymmetric and symmetric stretching at 1700 and 1660 cm^{-1}, respectively. The characterization data are in good agreement with the literature (Song et al., 2010; Chen et al., 2014; Dong et al., 2016).

The electrochemical performance of PI electrodes was also tested in electrolyte solutions of saturated $NaClO_4$, as shown in **Figure 7**. CV measurements were done at a scan rate of 0.1 mV/sec for the initial 20 cycles in the voltage window of 0 to −1.0 V vs. Ag/Ag_2SO_4; redox peaks related to reversible enolization of carbonyl groups in the PI moieties within this low voltage range are shown with no observation of hydrogen evolution. A high capacity of 160 mAh/g is observed in the initial cathodic scan, which is due to association of nearly two Na^+ ions at the carbonyl groups of PI (as shown in **Scheme 1**). After the first cycle, the discharge capacity is somewhat lower at 152 mAh/g. The retention of capacity is 91.3% with a coulombic efficiency of 99% at the end of 20 cycles at 0.1 mV/s. The better conjugation of this PI derivative results in high electronic conductivity as concluded based on DFT calculation (Andrzejak et al., 2000).

As was clearly studied for different PI derivatives like PMDA and NTCDA for lithium ion batteries by Song *et al.*, highly stable electrochemical performance was observed for the NTCDA derivative in nonaqueous media for Li ion batteries with reversible capacity of 173 mAh/g at C/5 rate (Song et al., 2010).

After completion of 20 cycles at 0.1 mV/sec, the scan rate was changed to 0.5 mV/sec. The obtained discharge capacity was 123 mAh/g and shows a stable reversible capacity of 115 mAh/g up to 50 cycles within the potential range of 0 to −1 V vs. Ag/Ag_2SO_4. The cycling efficiency reached was around 100%, as shown in **Figure 8A,B**. We attribute the stable capacity of PI at a fast scan rate with 100% coulombic efficiency not only to intrinsic properties of

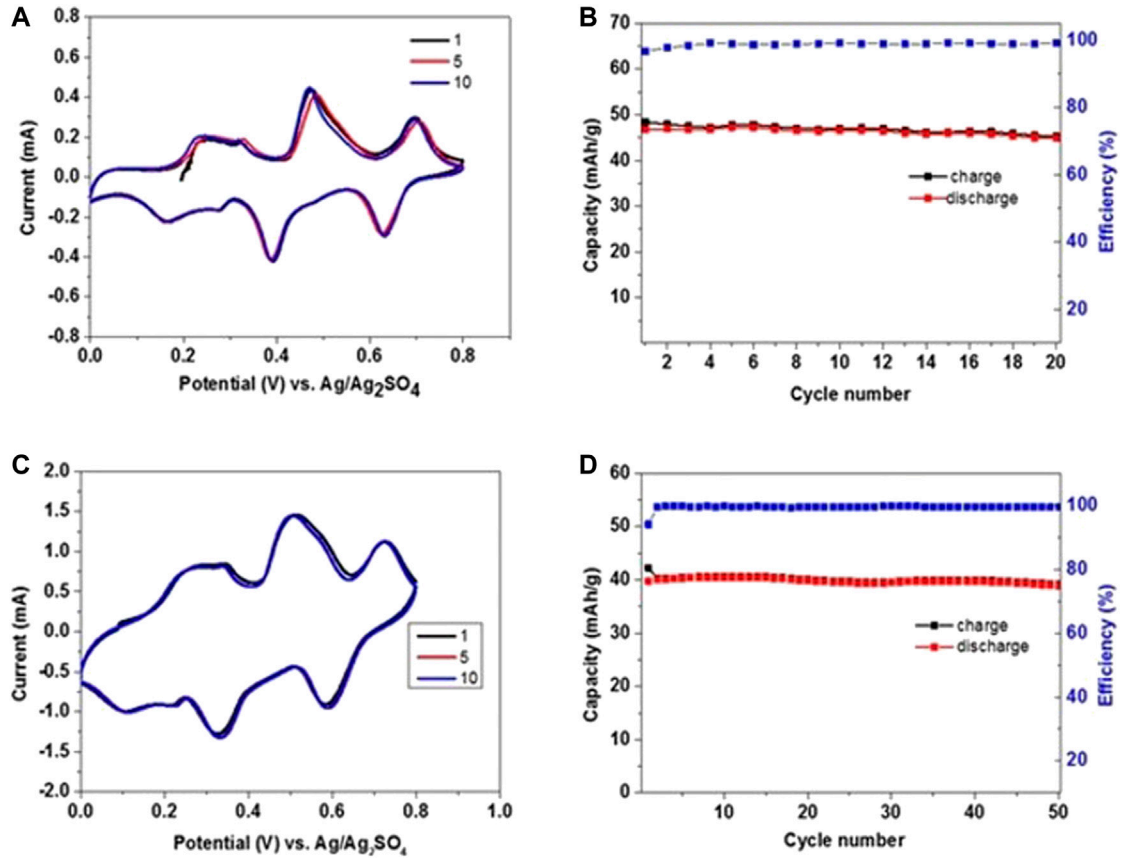

FIGURE 5 | CVs of NMO electrodes in saturated $NaClO_4$ electrolyte solution. The counter electrode comprised activated carbon and the reference electrode was Ag/Ag_2SO_4 **(A)** A scan rate of 0.1 mV/s for 20 cycles in the voltage window of 0–0.8 V vs. Ag/Ag_2SO_4 and **(B)** corresponding charge and discharge values during repeated anodic and cathodic cycling. **(C)** The scan rate is changed to 0.5 mV/s after 20 cycles within the same voltage range. **(D)** Charge and discharge values up to 50 cycles at 0.5 mV/s.

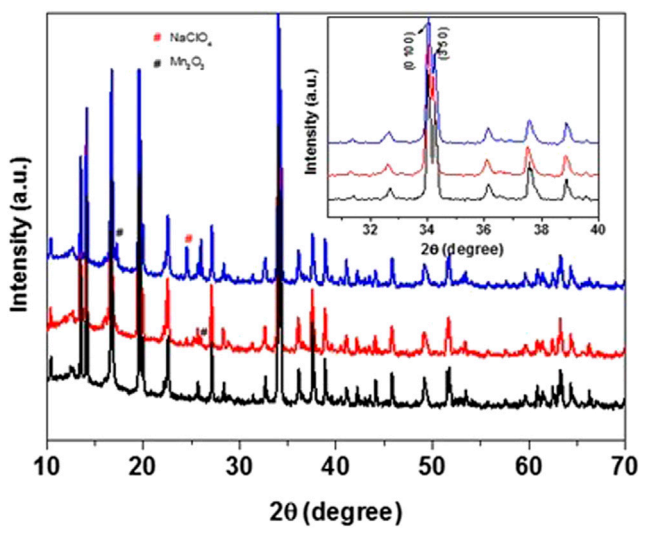

FIGURE 6 | Powder XRD patterns of NMO samples: untreated (black) and heat-treated (60°C for one week) in 8 m (red) and saturated (blue) $NaClO_4$ electrolyte solutions.

the active mass but also to the unique structure of the composite electrodes we used, which involved graphene as a conductive agent and the favorable use of saturated electrolyte solution. The effect of conductive additives like graphite and graphene or CNTs for enhancement of performance is well-known for nonaqueous and aqueous systems (Huang et al., 2018; Khamsanga et al., 2019). Potassium-organic batteries with pure PI and composites of acetylene black/PI and graphite/PI showed very poor capacity retention with the conductive additive acetylene black and 83% retention of capacity after 500 cycles for graphite/PI composite (Hu et al., 2019). Likewise, the graphene additive in our study contributed to the stable PI behavior during anodic and cathodic scan with low polarization.

Analysis of Full Cells Comprising $Na_{0.44}MnO_2$ Cathodes, PI Anodes, and Saturate Aqueous $NaClO_4$ Solution

The electrochemical performance of full cells containing cathodes comprising NMO and anodes comprising PI the active masses (respectively) in saturated aqueous $NaClO_4$

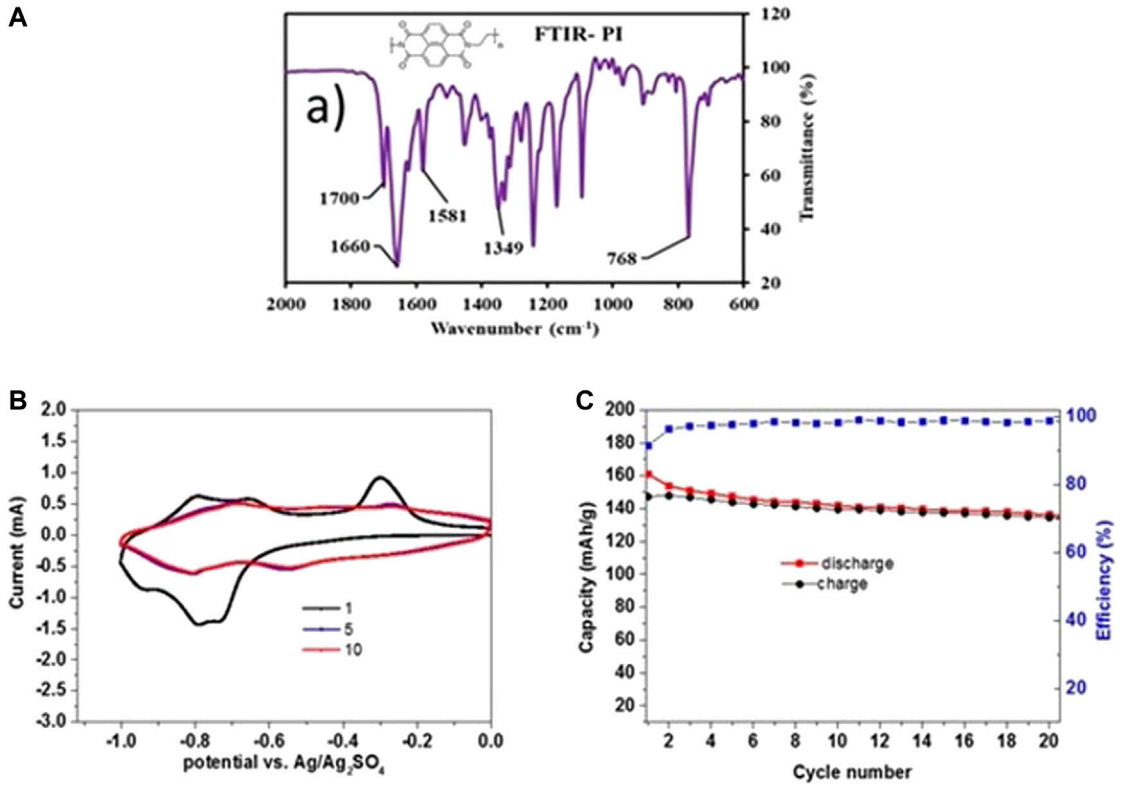

FIGURE 7 | (A) A FTIR spectrum of synthesized PI polymer (the insert shows the PI structure). **(B)** CVs were measured in saturated $NaClO_4$ electrolyte solutions with electrodes comprising PI as the active mass (the working electrodes, WE) and counter electrodes (CE) comprising NMO in excess, in three-electrodes cells at a scan rate of 0.1 mV/s in the voltage window of 0 to −1.0 V vs. Ag/Ag_2SO_4 (reference electrode) **(C)** Charge and discharge capacity values and cycling efficiency (as marked).

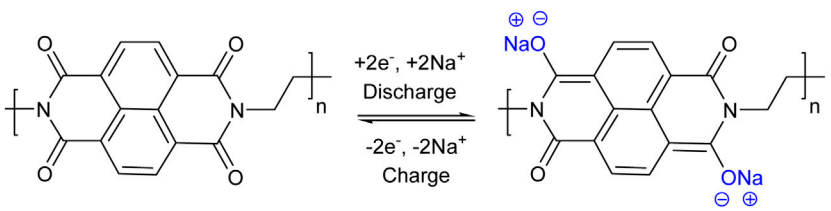

Scheme 1 | Redox reactions of PI anode in saturated $NaClO_4$ aqueous electrolyte solution.

electrolyte solution was characterized. The operation described schematically in **Figure 9** includes reversible Na ion de-insertion from NMO and its oxidation upon charging. In this stage, the PI is being coherently reduced in parallel and interacts with Na ions. In the spontaneous discharge process, sodium ions are inserted into the NMO cathode through a reduction process (through the external electricity flow of the battery) and the Na ions are desorbed from the PI (the PI is oxidized). This is a classical "rocking chair" mechanism, somewhat similar to that which works in Li ion batteries. The active sodium ions are initially included in the cathode. The charge step moves the ions from the cathode to the anode while the discharge processes return them back to the NMO cathode. With such a mechanism, the electrolyte solution's role is only to serve as thin ions conveyer between the electrodes. Hence, a minimal amount of electrolyte solution is needed for appropriate cell's operation, which helps to optimize the cells' parameters (specific capacity and energy density). Based on the characterization of the electrodes in half cells (voltammetric measurements, **Figure 5** and **Figure 8**), the balanced weight ratio between the cathode and the anode was around 3.0.

In order to confirm the validity of the cells' balance, galvanostatic experiments of three-electrodes' cells were carried out at 2C rate for up to 15 cycles, in which both electrodes could be measured in parallel. Stable performance

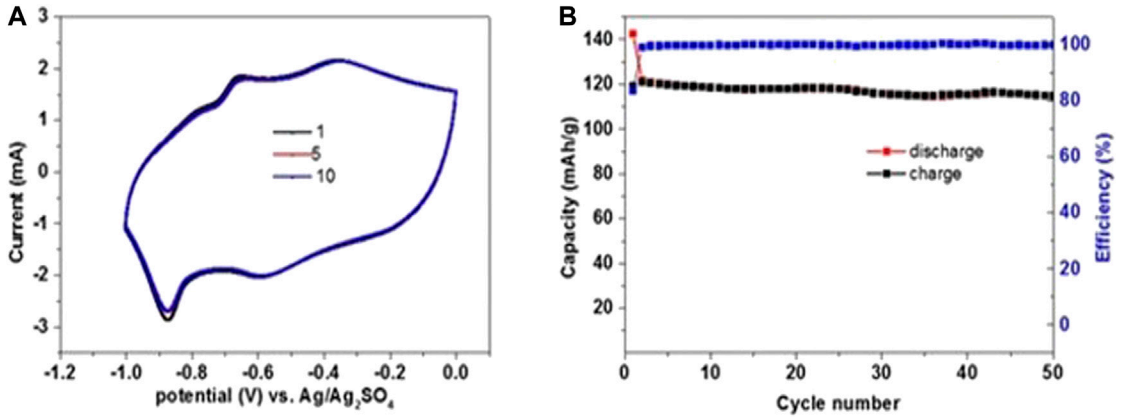

FIGURE 8 | (A) CVs of PI electrodes in 3 electrodes' cells, using counter electrodes containing excess of NMO and Ag/Ag_2SO_4 reference electrodes in saturated $NaClO_4$ electrolyte solution, scanning at 0.1 mV/s for 20 cycles (presented in Figure 7B) and then scanned at 0.5 mV/s in the voltage window of 0 to −1.0 V. **(B)** Charge (black) and discharge (red) capacities during anodic and cathodic scans at 0.5 mV/s up to 50 cycles, respectively, and cycling efficiency (blue).

was noticed for both NMO and PI electrodes (as can be seen in the supporting information, SI, **Supplementary Figure S1**). **Figure 10A** shows the rate capability for NMO/PI full cells operating galvanostatically in the voltage range of 0–1.7 V at a current rate of C/2, 1C, 2C, 5C, and 10C, up to six cycles at each rate. The corresponding stable discharge capacity values are 43, 41, 40, 36, and 28 mAh/g, respectively. The capacity is well retained upon cycling at 1C rate, as shown in **Figure 10A**. The charge–discharge profiles at different current rates are shown in **Figure 10B**. A stable capacity of 28 mAh/g (a reasonable value for such systems) is observed even at 10C rate, indicating the fast kinetics of both $Na_{0.44}MnO_2$ and PI electrodes in saturated aqueous $NaClO_4$ solution. As reported by Bu *et al.*, faster ionic and charge transfer kinetics was demonstrated in water-in-salt (WIS)-based electrolytes (17 m $NaClO_4$) for carbon-based supercapacitors (Bu et al., 2019). The voltage profiles of the cells show three inflections (degenerated plateaus) during charge/discharge reflecting properly the de-intercalation and intercalation processes of Na ions with the NMO as apparent from the CVs in **Figure 4** and **Figure 5**. The stability of these cells was further analyzed by subjecting them to prolonged cycling at different rates of C/2, 2C, and 5C, as presented in **Figure 11** and **Figure 12**. Average discharge capacities of 43.5, 41, and 35 mAh/g after 100, 430, and 2400 cycles, respectively, exhibit a reasonable stability. The efficiency was 96 and 98.8% at current rates of C/2 and 2C, respectively. The retention of capacity was 99.9% after 430 cycles at 2C rate (**Figure 11B**).

The charge and discharge voltage profiles per cycle nearly overlap during cycling at a fast 5C rate during prolonged cycling, as shown in **Figure 12B** for different cycles. These voltage profiles indicated no ohmic resistance during Na ion insertion and de-insertion in both electrodes. The discharge capacity was around 34 mAh/g with retention of 89.8% after 2,400 prolonged cycles with a coulombic efficiency of nearly 100% (see **Figure 12C**). The average voltage of 1.0 V was achieved for full cells with energy density around 24 Wh/kg, calculated based on the active materials weight of both PI and NMO electrodes. The prolonged cycling stability of 100%, indicating no water decomposition, may suggest the formation of metastable situation at the electrodes surfaces, thanks to the high concentration of the electrolyte solutions. The metastability leads to high overvoltage for releasing hydrogen and oxygen at the electrodes. A study of cells comprising $Na_{0.66}[Mn_{0.66}Ti_{0.34}]O_2$ cathode and $NaTi_2(PO_4)_3$ anode examined the advantage of WIS electrolyte, over conventional salt-in-water (SIW) solution using 1 M Na_2SO_4 solution. A high efficiency of 99.2% with better cycling stability and capacity retention was achieved with WIS, compared to

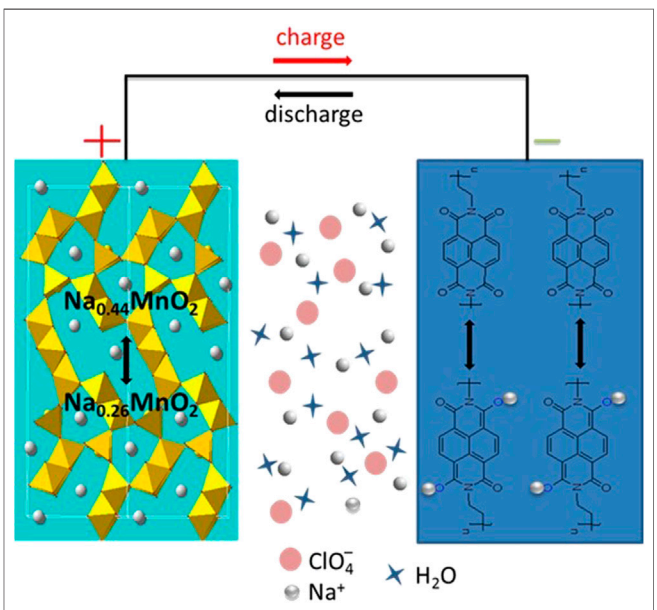

FIGURE 9 | A description of aqueous Na-ion battery with tunnel-type $Na_{0.44}MnO_2$ cathode and PI anode.

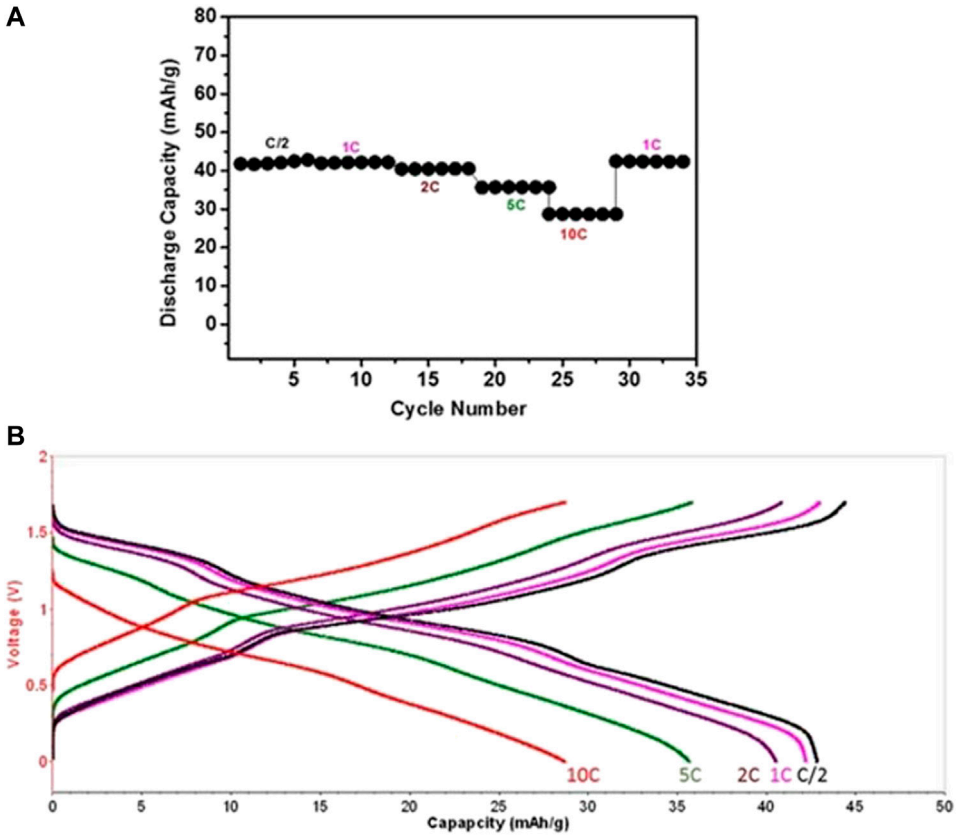

FIGURE 10 | (A) Representative plot of capacity vs. cycle number of balanced NMO-PI/saturated aqueous $NaClO_4$ electrolyte solution full cells operating galvanostatically between 0 and 1.7 V at C/2, 1C, 2C, 5C, and 10C (six cycles at each rate). **(B)** Corresponding sixth cycle charge–discharge voltage profiles of these full cells at different rates. 1C meaning a current density adjusted for full charge and discharge process within 1 h.

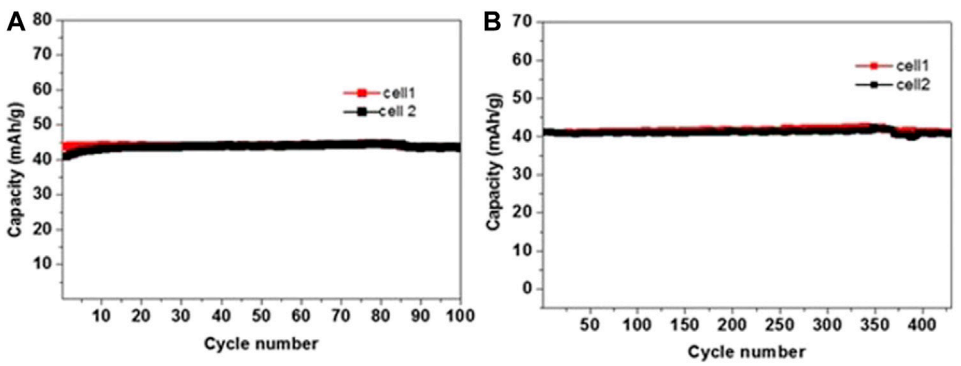

FIGURE 11 | Representative plots of discharge capacity for NMO-PI/saturated $NaClO_4$ solution full cells in long-term galvanostatic experiments, operating in the 0–1.7 V range at **(A)** C/2 and **(B)** 2C rate. The reproducibility is demonstrated by showing results from 2 cells in parallel experiments.

parallel experiments with 1 m Na_2SO_4 (SIW) solutions (Suo et al., 2017).

The effect of using saturated electrolyte solutions on the capacity losses and voltage fading of the cells described herein due to possible side reaction and material degradation processes was investigated by self-discharge analysis. Charged cells were held in solutions during several days and their OCV was measured, as presented in **Figure 13**. Initially, the cells were subjected to 10 cycles at 1C rate within the voltage window of 0–1.7 V, then charged at 1.7 V, and the voltage change was monitored. After four days, the cells were discharged to 0 V before undergoing five additional cycles. As shown in **Figure 13B**, the discharge capacity loss was 10.8% after four days

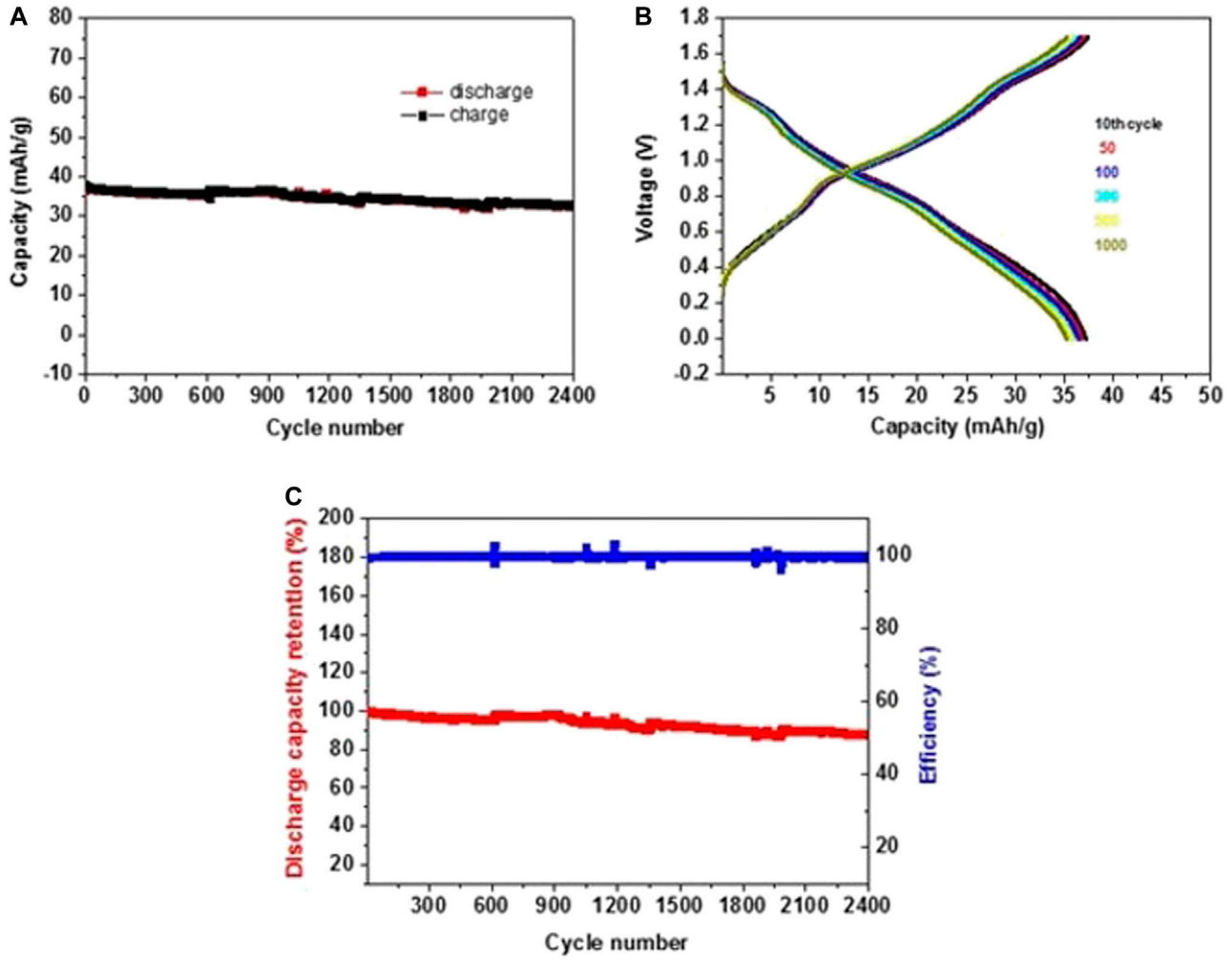

FIGURE 12 | (A) Galvanostatic charge–discharge capacity vs. cycle number at 5 C rate for NMO-PI/saturated $NaClO_4$ solution full cells operating in the range 0–1.7 V. **(B)** Charge–discharge profiles for different cycles. **(C)** Discharge capacity retention (red) and cycling efficiency (blue) vs. cycle number.

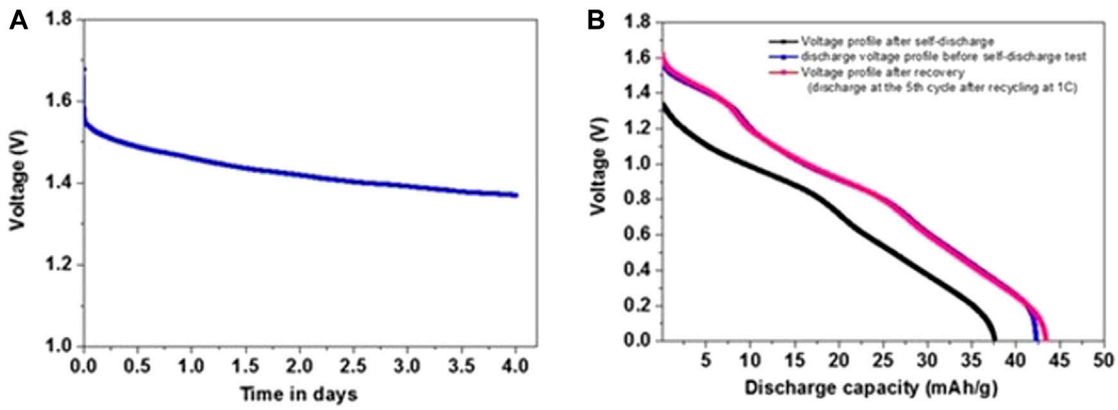

FIGURE 13 | (A) OCV changes of charged NMO/PI full cells held at 1.7 V after being cycled at 1C rate 10 times. **(B)** Representative discharge voltage-capacity profiles of these cells before the self-discharge experiment (in blue) and after being held at the charged state during 4 days in order to measure their self-discharge (black). The voltage profile in pink belongs to a typical discharge process (fifth cycle) of these cells upon their recycling after the end of the self-discharge experiment (storing the charged cells at OCV during 4 days).

at a charged state. The capacity could be fully recovered upon cycling after the self-discharge testing, as reflected in **Figure 13B**. These results indicate that the observed self-discharge is not related to any degradation of the electrodes. It can relate to current leaks in the cells. This phenomenon is still being explored.

CONCLUSION

In summary, $Na_{0.44}MnO_2$/polyimide (NMO/PI) aqueous Na ion batteries with high capacity retention for large energy storage applications were presented. The electrochemical performance of the tunnel-type NMO cathodes was studied in three-electrode cells. Low Mn ions dissolution from these cathodes was observed when saturated $NaClO_4$ electrolyte solution was used. A deliverable capacity of 38 mAh/g and a coulombic efficiency of 100% could be achieved for these NMO cathodes in the saturated solution, compared to the performance in 8 m $NaClO_4$ solution, a deliverable capacity of 29 mAh/g. The PI derivative showed excellent stability in the low potential range and a reversible capacity of 115 mAh/g could be obtained in the saturated electrolyte solutions.

Full cells with NMO cathodes and PI derivative anodes, with appropriate mass balance that takes into account the specific capacities ratio of the electrodes, were composed and tested. The NMO/PI full cells can operate at a voltage span of 1.7 V, delivering capacities of 43, 41, 35, and 28 mAh/g-cathode at C/2, 2C, 5C, and 10C, respectively. The fast rate capability of these full cells may result from better ionic and charge transfer kinetics that can be reached in the saturated $NaClO_4$ solutions. During 2,400 cycles at 5C rates, these cells demonstrated a capacity of 33 mAh/g-cathode with fully reversible charge and discharge voltage profiles, and a negligible ohmic drop. These cycling results indicate no dissolution of cations from the cathodes or any degradation of both electrodes during cycling. The low ohmic resistance means a very low hysteresis between the charge and discharge processes. The important consequence of that is excellent energy efficiency per cycle, which makes these systems really suitable for large energy storage. In prolonged cycling experiments, the capacity retention of these cells was nearly 90% with a coulombic efficiency of 100% after 2,400 cycles.

The high stability of the electrode materials without degradation and their interactions in saturated electrolyte media were further confirmed by maintaining cells at their charged state, namely, 1.7 V during several days. While showing 10% discharge capacity loss, upon resuming their cycling, a full capacity recovery and retention was demonstrated.

These cells comprise environmentally friendly and low-cost manganese oxides and organic-based materials, containing most abundant elements. Hence, we have demonstrated highly stable aqueous Na-ion battery technology, the rate capability and energy efficiency of which are excellent, which in turn makes it very suitable for large energy storage applications. Using highly concentrated electrolyte solutions for these systems helped to reach this high performance.

DATA AVAILABILITY STATEMENT

The original contributions presented in the study are included in the article/**Supplementary Material**, further inquiries can be directed to the corresponding author.

AUTHOR CONTRIBUTIONS

SM, AN, SL, and DA conceived the idea, designed experiments, and analyzed data. AN synthesized organic polyimide for anode material. SM analyzed data and wrote the manuscript. All authors contributed to the discussion.

FUNDING

A partial support for this work was obtained from the Israeli Ministry of Energy, from the Israeli Prime-Minister office, and the Israeli Committee for High Education (CHE) in the framework of the INREP project.

SUPPLEMENTARY MATERIAL

The Supplementary Material for this article can be found online at: https://www.frontiersin.org/articles/10.3389/fenrg.2020.615677/full#supplementary-material.

REFERENCES

Andrzejak, M., Mazur, G., and Petelenz, P. (2000). Quantum chemical results as input for solid state calculations: charge transfer states in molecular crystals. *J. Mol. Struct.* 527, 91–102. doi:10.1016/S0166-1280(00)00481-4

Armand, M., and Tarascon, J.-M. (2008). Building better batteries. *Nature* 451, 652–657. doi:10.1038/451652a

Barbieri, O., Hahn, M., Herzog, A., and Kötz, R. (2005). Capacitance limits of high surface area activated carbons for double layer capacitors. *Carbon N. Y.* 43, 1303–1310. doi:10.1016/j.carbon.2005.01.001

Bhosale, M. E., Chae, S., Kim, J. M., and Choi, J. Y. (2018). Organic small molecules and polymers as an electrode material for rechargeable lithium ion batteries. *J. Mater. Chem. A.* 6, 19885–19911. doi:10.1039/c8ta04906h

Bin, D., Wang, F., Tamirat, A. G., Suo, L., Wang, Y., Wang, C., et al. (2018). Progress in aqueous rechargeable sodium-ion batteries. *Adv. Energy Mater.* 8, 1–31. doi:10.1002/aenm.201703008

Brandt, A., and Balducci, A. (2014). Theoretical and practical energy limitations of organic and ionic liquid-based electrolytes for high voltage electrochemical double layer capacitors. *J. Power Sources* 250, 343–351. doi:10.1016/j.jpowsour.2013.10.147

Brandt, A., Pires, J., Anouti, M., and Balducci, A. (2013). An investigation about the cycling stability of supercapacitors containing protic ionic liquids as electrolyte components. *Electrochim. Acta.* 108, 226–231. doi:10.1016/j.electacta.2013.06.118

Bu, X., Su, L., Dou, Q., Lei, S., and Yan, X. (2019). A low-cost "water-in-salt" electrolyte for a 2.3 V high-rate carbon-based supercapacitor. *J. Mater. Chem. A.* 7, 7541–7547. doi:10.1039/c9ta00154a

Cao, X., Wang, L., Chen, J., and Zheng, J. (2018). A low-cost Mg2+/Na+ hybrid aqueous battery. J. Mater. Chem. A6, . 15762–15770. doi:10.1039/c8ta04930k

Chen, L., Bao, J. L., Dong, X., Truhlar, D. G., Wang, Y., Wang, C., et al. (2017). Aqueous Mg-ion battery based on polyimide anode and Prussian blue cathode. *ACS Energy Lett.* 2, 1115–1121. doi:10.1021/acsenergylett.7b00040

Chen, L., Li, W., Guo, Z., Wang, Y., Wang, C., Che, Y., et al. (2015). Aqueous lithium-ion batteries using O_2 self-elimination polyimides electrodes. *J. Electrochem. Soc.* 162, A1972–A1977. doi:10.1149/2.0101510jes

Chen, L., Li, W., Wang, Y., Wang, C., and Xia, Y. (2014). Polyimide as anode electrode material for rechargeable sodium batteries. *RSC Adv.* 4, 25369–25373. doi:10.1039/c4ra03473b

Comte, A. L., Chhin, D., Gagnon, A., Retoux, R., Brousse, T., and Belanger, D. (2015). Spontaneous grafting of 9,10-phenanthrenequinone on porous carbon as an active electrode material in an electrochemical capacitor in an alkaline electrolyte. *J. Mater. Chem. A.* 3, 6146–6156. doi:10.1039/c4ta05536e

Dall'Asta, V., Buchholz, D., Chagas, L. G., Dou, X., Ferrara, C., Quartarone, E., et al. (2017). Aqueous processing of $Na_{0.44}MnO_2$ cathode material for the development of greener Na-ion batteries. *ACS Appl. Mater. Interfaces.* 9, 34891–34899. doi:10.1021/acsami.7b09464

Dong, X., Chen, L., Liu, J., Haller, S., Wang, Y., and Xia, Y. (2016). Environmentally-friendly aqueous Li (or Na)-ion battery with fast electrode kinetics and super-long life. *Sci. Adv.* 2, 1–9. doi:10.1126/sciadv.1501038

Evanko, B., Yoo, S. J., Lipton, J., Chun, S. E., Moskovits, M., Ji, X., et al. (2018). Stackable bipolar pouch cells with corrosion-resistant current collectors enable high-power aqueous electrochemical energy storage. *Energy Environ. Sci.* 11, 2865–2875. doi:10.1039/c8ee00546j

Gheytani, S., Liang, Y., Jing, Y., Xu, J. Q., and Yao, Y. (2016). Materials chemistry A. *J. Mater. Chem. A.* 4, 395–399. doi:10.1039/c5ta07366a

Haüpler, B., Rössel, C., Schwenke, A. M., Winsberg, J., Schmidt, D., Wild, A., et al. (2016). Aqueous zinc-organic polymer battery with a high rate performance and long lifetime. *NPG Asia Mater.* 8, e283. doi:10.1038/am.2016.82

Hernández, G., Casado, N., Zamarayeva, A. M., Duey, J. K., Armand, M., Arias, A. C., et al. (2018). Perylene polyimide-polyether anodes for aqueous all-organic polymer batteries. *ACS Appl. Energy Mater.* 1, 7199–7205. doi:10.1021/acsaem.8b01663

Hu, Y., Ding, H., Bai, Y., Liu, Z., Chen, S., Wu, Y., et al. (2019). Rational design of a polyimide cathode for a stable and high-rate potassium-ion battery. *ACS Appl. Mater. Interfaces* 11, 42078–42085. doi:10.1021/acsami.9b13118

Huang, Y., Liu, J., Huang, Q., Zheng, Z., Hiralal, P., Zheng, F., et al. (2018). Flexible high energy density zinc-ion batteries enabled by binder-free MnO_2/reduced graphene oxide electrode. *npj Flex. Electron.* 21, 1–6. doi:10.1038/s41528-018-0034-0

Kang, J., Lim, T., Jeong, M. H., and Suk, J. W. (2019). Graphene papers with tailored pore structures fabricated from crumpled graphene spheres. *Nanomaterials* 9, 815. doi:10.3390/nano9060815

Khamsanga, S., Pornprasertsuk, R., Yonezawa, T., Mohamad, A. A., and Kheawhom, S. (2019). δ-MnO2 nanoflower/graphite cathode for rechargeable aqueous zinc ion batteries. *Sci. Rep.* 9, 8441. doi:10.1038/s41598-019-44915-8

Kim, D., Shin, G., Kang, Y. J., Kim, W., and Ha, J. S. (2013). Fabrication of a stretchable solid-state micro-supercapacitor array. *ACS Nano* 7, 7975–7982. doi:10.1021/nn403068d

Kim, H., Hong, J., Park, K. Y., Kim, H., Kim, S. W., and Kang, K. (2014). Aqueous rechargeable Li and Na ion batteries. *Chem. Rev.* 114, 11788–11827. doi:10.1021/cr500232y

Lee, M. H., Kim, S. J., Chang, D., Kim, J., Moon, S., Oh, K., et al. (2019). Toward a low-cost high-voltage sodium aqueous rechargeable battery. *Mater. Today.* 29, 26–36. doi:10.1016/j.mattod.2019.02.004

Li, L., Wu, Z., Yuan, S., and Zhang, X. B. (2014a). Advances and challenges for flexible energy storage and conversion devices and systems. *Energy Environ. Sci.* 7, 2101–2122. doi:10.1039/c4ee00318g

Li, X., Zhu, X., Liang, J., Hou, Z., Wang, Y., Lin, N., et al. (2014b). Graphene-supported $NaTi_2(PO_4)_3$ as a high rate anode material for aqueous sodium ion batteries. *J. Electrochem. Soc.* 161, A1181–A1187. doi:10.1149/2.0081409jes

Li, N., Chen, Z., Ren, W., Li, F., and Cheng, H. M. (2012). Flexible graphene-based lithium ion batteries with ultrafast charge and discharge rates. *PNAS.* 109, 17360–17365. doi:10.1073/pnas.1210072109

Li, S. (2017). Electrochemical stability of aluminum current collector in aqueous rechargeable lithium-ion battery electrolytes. *J. Appl. Electrochem.* 47, 839–853. doi:10.1007/s10800-017-1081-2

Li, S. Y., and Church, B. C. (2016). Effect of aqueous-based cathode slurry pH and immersion time on corrosion of aluminum current collector in lithium-ion batteries. *Mater. Corros.* 67, 978–987. doi:10.1002/maco.201608843

Li, W., Zhang, F., Xiang, X., and Zhang, X. (2017). High-efficiency Na-storage performance of a nickel-based ferricyanide cathode in high-concentration electrolytes for aqueous sodium-ion batteries. *ChemElectroChem* 4, 2870–2876. doi:10.1002/celc.201700776

Lim, H., Jung, J. H., Park, Y. M., Lee, H. N., and Kim, H. J. (2018). High-performance aqueous rechargeable sulfate- and sodium-ion battery based on polypyrrole-MWCNT core-shell nanowires and $Na_{0.44}MnO_2$ nanorods. *Appl. Surf. Sci.* 446, 131–138. doi:10.1016/j.apsusc.2018.02.021

Luo, J., Cui, W., He, P., and Xia, Y. (2010). Raising the cycling stability of aqueous lithium-ion batteries by eliminating oxygen in the electrolyte. *Nat. Chem.* 2, 760–765. doi:10.1038/nchem.763

Malka, D., Giladi, S., Hanna, O., Weitman, M., Cohen, R., Elias, Y., et al. (2019). Catechol-modified carbon cloth as hybrid electrode for energy storage devices. *J. Electrochem. Soc.* 166, A1147–A1153. doi:10.1149/2.0911906jes

Pang, G., Nie, P., Yuan, C., Shen, L., Zhang, X., Zhu, J., et al. (2014). Enhanced performance of aqueous sodium-ion batteries using electrodes based on the $NaTi_2(PO_4)_3$/MWNTs-$Na_{0.44}MnO_2$ system. *Energy Technol.* 2, 705–712. doi:10.1002/ente.201402045

Pognon, G., Brousse, T., and Bélanger, D. (2011). Effect of molecular grafting on the pore size distribution and the double layer capacitance of activated carbon for electrochemical double layer capacitors. *Carbon* 49, 1340–13488. doi:10.1016/j.carbon.2010.11.055

Pognon, G., Cougnon, C., Mayilukila, D., and Bélanger, D. (2012). Catechol-modified activated carbon prepared by the diazonium chemistry for application as active electrode material in electrochemical capacitor. *ACS Appl. Mater. Interfaces.* 4, 3788–3796. doi:10.1021/am301284n

Poonam, S., Sharma, K., Arora, A., and Tripathi, S. K. (2019). Review of supercapacitors: materials and devices. *J. Energy Storage.* 21, 801–825. doi:10.1016/j.est.2019.01.010

Sadeghi, S., and Javaran, E. J. (2019). Comparison of combining redox flow and lead-acid batteries with On-grid and stand-alone photovoltaic systems. *Environ. Prog. Sustain. Energy* 38, 1–10. doi:10.1002/ep.13182

Sauvage, F., Laffont, L., Tarascon, J. M., and Baudrin, E. (2007). Study of the insertion/deinsertion mechanism of sodium into $Na_{0.44}MnO_2$. *Inorg. Chem.* 46, 3289–3294. doi:10.1021/ic0700250

Shao, J., Li, X., Qu, Q., and Wu, Y. (2013). Study on different power and cycling performance of crystalline $K_xMnO_2{\cdot}nH_2O$ as cathode material for supercapacitors in Li_2SO_4, Na_2SO_4, and K_2SO_4 aqueous electrolytes. *J. Power Sources* 223, 56–61. doi:10.1016/j.jpowsour.2012.09.046

Shin, J., Seo, J. K., Yaylian, R., Huang, A., and Meng, Y. S. (2020). A review on mechanistic understanding of MnO_2 in aqueous electrolyte for electrical energy storage systems. *Int. Mater. Rev.* 65, 356–387. doi:10.1080/09506608.2019.1653520

Simon, P., and Gogotsi, Y. (2008). Materials for electrochemical capacitors. *Nat. Mater.* 7, 845–854. doi:10.1038/nmat2297

Song, W. J., Park, J., Kim, D. H., Bae, S., Kwak, M. J., Shin, M., et al. (2018). Jabuticaba-inspired hybrid carbon filler/polymer electrode for use in highly stretchable aqueous Li-ion batteries. *Adv. Energy Mater.* 8, 1–10. doi:10.1002/aenm.201702478

Song, Z., Zhan, H., and Zhou, Y. (2010). Polyimides: Promising energy-storage materials. *Angew. Chem. Int. Ed.* 49, 8444–8448. doi:10.1002/anie.201002439

Stoller, M. D., Park, S., Yanwu, Z., An, J., and Ruoff, R. S. (2008). Graphene-Based ultracapacitors. *Nano Lett.* 8, 3498–3502. doi:10.1021/nl802558y

Suo, L., Borodin, O., Wang, Y., Rong, X., Sun, W., Fan, X., et al. (2017). "Water-in-salt " electrolyte makes aqueous sodium-ion battery safe, green, and long-lasting. *Adv. Energy Mater.* 7, 1701189. doi:10.1002/aenm.201701189

Tang, C., Long, G., Hu, X., Wong, K.-W., Lau, W.-M., Fan, M., et al. (2014). Conductive polymer nanocomposites with hierarchical multi-scale structures via self-assembly of carbon-nanotubes on graphene on polymer-microspheres. *Nanoscale*, 6, 7877–7888. doi:10.1039/C3NR06056J

Tekin, B., Sevinc, S., Morcrette, M., and Demir-cakan, R. (2017). A new sodium-based aqueous rechargeable battery System: the special case of $Na_{0.44}MnO_2$/dissolved sodium polysulfide. *Energy technol.* 5, 2182–2188. doi:10.1002/ente.201700245

Toby, B. H. (2001). EXPGUI, a graphical user interface for GSAS. *Journal of Applied Crystallography* 2001 (34), 210. doi:10.1107/S0021889801002242

Wang, Y., Mu, L., Liu, J., Yang, Z., Yu, X., Gu, L., et al. (2015). A novel high capacity positive electrode material with tunnel-type structure for aqueous sodium-ion batteries. *Adv. Energy Mater.* 5, 1–8. doi:10.1002/aenm.201501005

Weissmann, M., Crosnier, O., Brousse, T., and Bélanger, D. (2012). Electrochemical study of anthraquinone groups, grafted by the diazonium chemistry, in different aqueous media-relevance for the development of aqueous hybrid electrochemical capacitor. *Electrochim. Acta.* 82, 250–256. doi:10.1016/j.electacta.2012.05.130

Wen, Y. H., Shao, L., Zhao, P. C., Wang, B. Y., Cao, G. P., and Yang, Y. S. (2017). Carbon coated stainless steel mesh as a low-cost and corrosion-resistant current collector for aqueous rechargeable batteries. *J. Mater. Chem. A.* 5, 15752–15758. doi:10.1039/c7ta03500d

Whitacre, J. F., Tevar, A., and Sharma, S. (2010). $Na_4Mn_9O_{18}$ as a positive electrode material for an aqueous electrolyte sodium-ion energy storage device. *Electrochem. commun.* 12, 463–466. doi:10.1016/j.elecom.2010.01.020

Xu, C., Du, H., Li, B., Kang, F., and Zeng, Y. (2009a). Asymmetric activated carbon-manganese dioxide capacitors in mild aqueous electrolytes containing alkaline-earth cations. *J. Electrochem. Soc.* 156, A435–A441. doi:10.1149/1.3106112

Xu, C., Du, H., Li, B., Kang, F., and Zeng, Y. (2009b). Reversible insertion properties of zinc ion into manganese dioxide and its application for energy storage. *Electrochem. Solid-State Lett.* 12, A61–A65. doi:10.1149/1.3065967

Yang, C., Ji, X., Fan, X., Gao, T., Suo, L., Wang, F., et al. (2017a). Flexible aqueous Li-ion battery with high energy and power densities. *Adv. Mater.* 29, 1–8. doi:10.1002/adma.201701972

Yang, J., Hu, C., Wang, H., Yang, K., Liu, J. B., and Yan, H. (2017b). Review on the research of failure modes and mechanism for lead–acid batteries. *Int. J. Energy Res.* 41, 336–352. doi:10.1002/er.3613

Yolshina, L. A., Yolshina, V. A., Yolshin, A. N., and Plaksin, S. V. (2015). Novel lead-graphene and lead-graphite metallic composite materials for possible applications as positive electrode grid in lead-acid battery. *J. Power Sources* 278, 87–97. doi:10.1016/j.jpowsour.2014.12.036

Yu, L., and Chen, G. Z. (2019). Ionic liquid-based electrolytes for supercapacitor and supercapattery. *Front. Chem.* 7, 1–15. doi:10.3389/fchem.2019.00272

Conflict of Interest: The authors declare that the research was conducted in the absence of any commercial or financial relationships that could be construed as a potential conflict of interest.